Three-dimensional diffuse optical tomography of bones and joints

Yong Xu
Nicusor Iftimia
Huabei Jiang
Clemson University
Biomedical Optics Laboratory
Department of Physics and Astronomy
Clemson, South Carolina 29634-0978

L. Lyndon Key
Medical University of South Carolina
Department of Pediatrics and
    General Clinical Research Center
Charleston, South Carolina 29425

Marcy B. Bolster
Medical University of South Carolina
Division of Rheumatology and Immunology
Charleston, South Carolina 29425

Abstract. We present for the first time full three-dimensional (3D) volumetric reconstruction of absorption images of *in vitro* and *in vivo* bones and joints from near-infrared tomographic measurements. Imaging experiments were conducted on human finger and chicken bones embedded in cylindrical scattering media using a Clemson multichannel diffuse optical imager. The volumetric optical images were recovered with our 3D finite element based reconstruction algorithm. Our results show that 3D imaging methods can provide details of the joint structure/composition that would be impossible from two-dimensional imaging methods. © *2002 Society of Photo-Optical Instrumentation Engineers.* [DOI: 10.1117/1.1427336]

1 Introduction

Near-infrared (NIR) diffuse optical tomography (DOT) has found its applications in imaging thick tissues such as breast and brain.[1–7] The idea of DOT is to extract the spatial maps of intrinsic tissue absorption and scattering coefficients from the measured optical data through model-based reconstruction methods. The spectra of these optical properties will then allow one to obtain tissue functional images such as hemoglobin, water content, and cellular structure. In DOT, an effective reconstruction algorithm is crucial. To date various linear and nonlinear reconstruction algorithms have been successfully tested and evaluated using considerable laboratory phantom measurements and initial clinical data from different hardware systems including continuous wave (cw), frequency, and time domain.[8–27]

DOT has been recently applied to image other tissues such as human joints and associated bones. This particular application of DOT was conceived theoretically by Klose et al.[28] and demonstrated experimentally by Xu et al.[29] very recently. Diseases related to bones and joints such as osteoporosis and arthritis are a major cause of morbidity in the population over 50, affecting more than 68 million Americans. Conventional imaging modalities including x-ray radiography, computed tomography, magnetic resonance imaging, and ultrasonography usually can provide only tissue structural information which limits their use especially for early detection of diseases.

In the work of Xu et al.,[29] we have shown that two-dimensional (2D) DOT images of *in vitro* and *in vivo* bones and joints can be quantitatively reconstructed using NIR tomographic measurements. Encouraged by this successful experience, in a separate study, we have applied DOT to image a patient with osteoarthritis (OA).[30] The findings from this study suggest that the diseased synovial membrane/fluid does show significant different optical properties compared to the

joints from two healthy volunteers. While we have evidenced the potential high sensitivity of DOT for detecting OA (based on the quantitative nature of optical images at the joints), we have also seen that some of the important small joint structures/compositions such as cartilage, blood vessels, and synovial membrane could not be clearly differentiated in these 2D images presented. In part we believe that it would be difficult for 2D imaging methods to capture these small components distributed between the two bones with a separation distance less than 1 mm. The strong three-dimensional (3D) scattering nature of the bones would affect the 2D joint imaging significantly. This necessitates our consideration of optical image reconstruction in a 3D framework.

While 3D optical image reconstructions have been primarily limited to simulations,[31–33] Jiang et al.[34] and Arridge et al.[35] have recently demonstrated full 3D reconstructions using breast or brain phantom model from cw and time-domain data, respectively. Assisted with ultrasound localization, Holboke et al.[36] have attempted to obtain a 3D optical characterization of the breast in a human subject with frequency-domain measurements. Most recently, Jiang et al.[37] have presented a full 3D reconstruction of absorption images of the human breast from cw measurements. In this paper we demonstrate for the first time that 3D volumetric absorption images of *in vitro* and *in vivo* bones and joints can be reconstructed using our DOT approach. The tomographic data were obtained with our automated multichannel DOT system, and the 3D images were recovered with our finite-element based nonlinear algorithm. The 3D images obtained show details of the joints/bones that are not available from the 2D images we achieved previously.

2 Materials and Methods

Our multichannel frequency-domain DOT imager has been described in detail.[26,29,34] Briefly, light from a 785 nm 50 mW

Address all correspondence to Huabei Jiang. Tel: 864-656-5307; Fax: 854-656-0805; E-mail: hjiang@clemson.edu
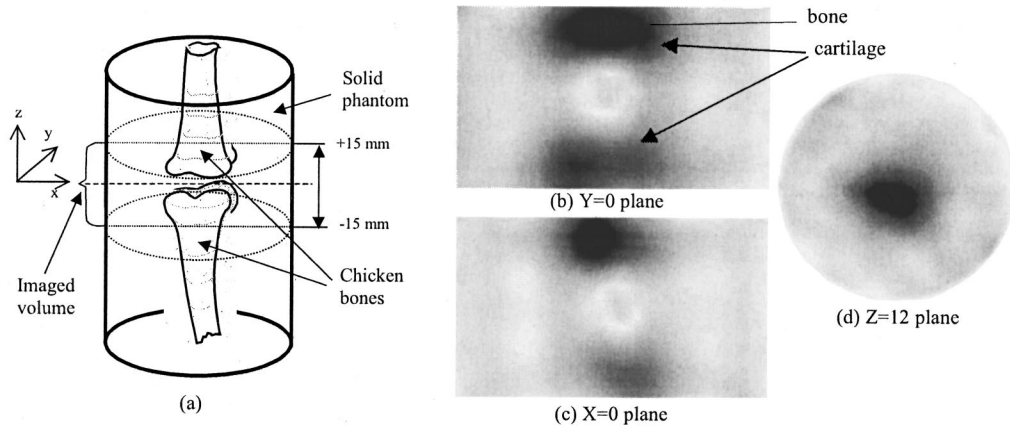
Fig. 1 (a) Schematic of the *in vitro* test configuration including the solid phantom, chicken bones, and measurement volume. (b), (c), and (d) Reconstructed absorption images at three cut-planes from phantom/bones measurements (the dark region corresponds to the bones; the gray background corresponds to the solid phantom).

diode laser (Thorlabs) is sequentially sent to the sample by sixteen 3 mm fiber optic bundles. For each source position, the diffused light is received at 16 detector positions along the surface of the sample and sequentially delivered to a photomultiplier tube (R928, Hamamatsu). The multiplexing of the source/detector fibers is accomplished by two automatic moving stages (17NST101, Melles-Griot). Data acquisition is realized by Labview routines (National Instruments). Both source and detector fiber bundles are firmly held by a metal ring structure with a diameter of 5 cm. Sixteen detector fiber bundles are arranged equally spaced around the annulus with another 16 source fiber bundles interspersed between the detector bundles. Tomographic data collection at multiple measurement planes are needed for 3D reconstruction. In the current configuration data collection time is about 10 min per measurement plane.

For the *in vitro* experiment, the sample consisted of two chicken bones embedded in a cylindrical solid phantom with a diameter of 5 cm. The solid phantom has contained a scattering medium composed of Intralipid (a fat emulsion suspension) with India ink as an absorber, which has had $\mu_a = 0.005 \, \text{mm}^{-1}$ (absorption coefficient) and $\mu_s' = 1.0 \, \text{mm}^{-1}$ (reduced scattering coefficient). Agar powders have been used to solidify the Intralipid/ink suspensions. A schematic of this phantom is given in Figure 1(a). The tomographic measurements have been conducted at three different planes. For the *in vivo* experiment, the sample was the index finger of a healthy volunteer inserted into the same cylindrical solid phantom (the protocol was approved by the institutional review board and written informed consent was obtained from the participant). Figure 2 displays a schematic of the finger measurement configuration. A translation stage coupled with a high precision digital scale was used to vertically position the ring holding the source and detector fibers. The *in vivo* tomographic measurements have been conducted also at three different planes.

The absorption image of the sample was recovered using our 3D nonlinear, finite element based reconstruction algorithm. This algorithm uses a regularized Newton's method to update an initial optical property distribution iteratively in or-

der to minimize an object function composed of a weighted sum of the squared difference between computed and measured optical data at the sample surface. The computed optical data (i.e., photon density) is obtained by solving the photon diffusion equation with the finite element method. The mathematical details of our 3D algorithm and its evaluation with phantom and *in vivo* breast tissues have been described elsewhere.[34,37] Briefly, the core procedure in our reconstruction algorithm is to iteratively solve the regularized matrix equation

$$(\mathfrak{J}^T\mathfrak{J} + \lambda I)\delta\chi = \mathfrak{J}^T[\Phi^{(m)} - \Phi^{(c)}], \qquad (1)$$

where $\mathfrak{J}$ is the Jacobian matrix that should be formed by $\partial\Phi/\partial D$ and $\partial\Phi/\partial\mu_a$ at the boundary measurement sites; Φ is the photon density; μ_a is the absorption coefficient; D is the diffusion coefficient which can be written as $D = 1/3\mu_s'$, where μ_s' is the reduced scattering coefficient. I is the identity matrix and λ can be a scalar or a diagonal matrix. $\Delta\chi$
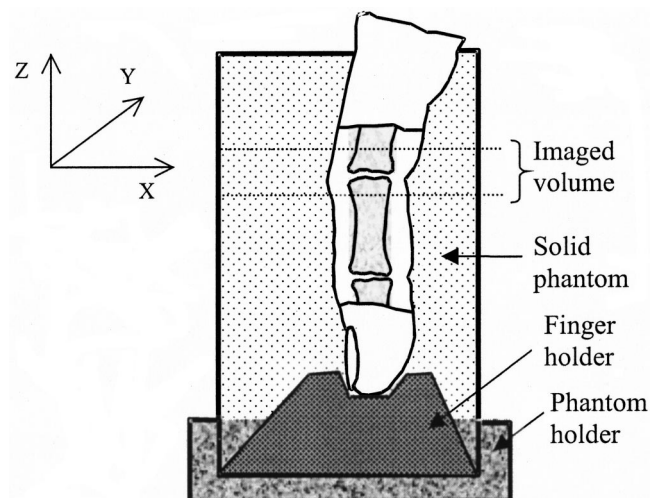

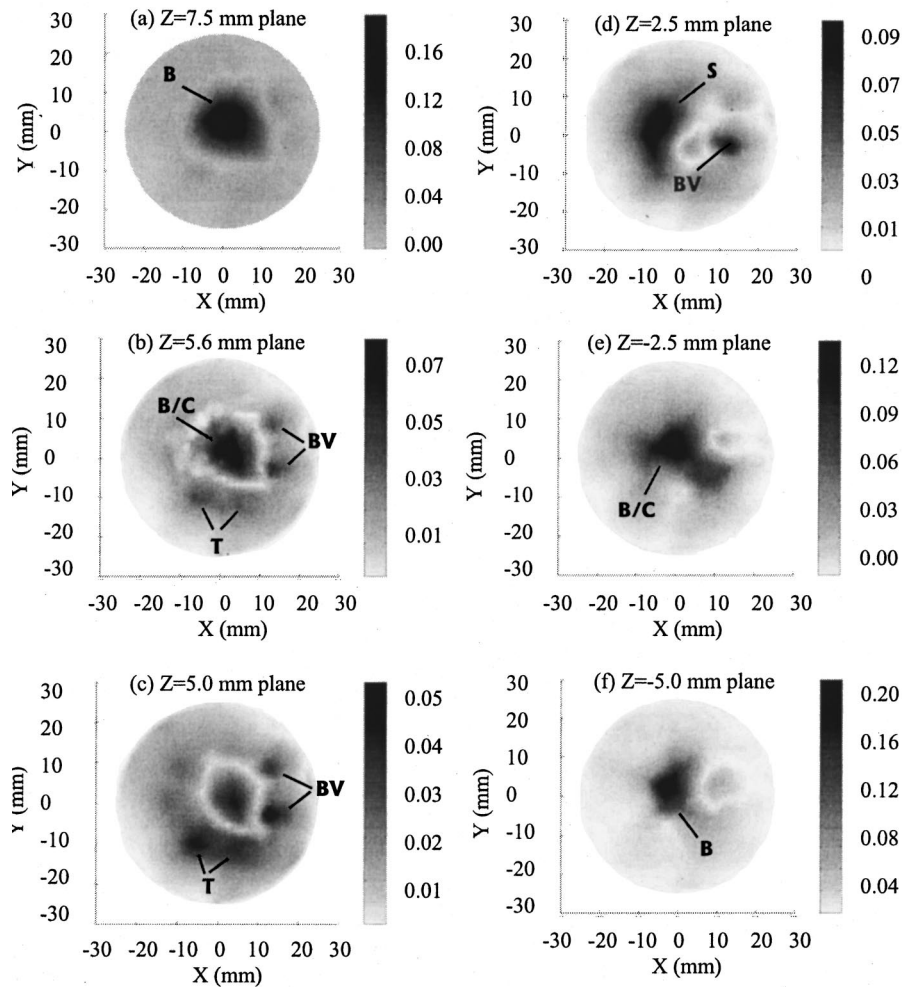**Fig. 2** Schematic of the finger measurement configuration.

Fig. 3 Transverse slices of reconstructed absorption images from *in vivo* measurements obtained around the proximal interphalangeal (PIP) joint of the index finger (the dark region corresponds to the finger; the gray background corresponds to the solid phantom). The axes (left and bottom) illustrate the spatial scale, in millimeters, whereas the gray scale (right) records the absorption coefficient, in inverse millimeters. *B*: bone; *B/C*: bone/cartilage; *BV*: blood vessel; *T*: tendon; *S*: synovium.

$=(\Delta D_1,\Delta D_2,\cdots,\Delta D_N,\Delta\mu_{a,1},\Delta\mu_{n,2},\cdots,\Delta\mu_{a,N})^T$ is the update vector for the optical property profiles, where N is the total number of nodes in the finite element mesh used; $\Phi^{(m)} =[\Phi_1^{(m)},\Phi_2^{(m)},\cdots,\Phi_M^{(m)}]$ and $\Phi^{(c)}=[\Phi_1^{(c)},\Phi_2^{(c)},\cdots,\Phi_M^{(c)}]$ where $\Phi_i^{(m)}$ and $\Phi_i^{(c)}$, respectively, are measured and calculated data for $i=1,2,...,M$ boundary locations.

In DOT, the goal is to update the μ_a and D or μ_s' distributions through the iterative solution of Eq. (1) so that a weighted sum of the squared difference between computed and measured data can be minimized. To generate the 3D images within 3.0 cm height from *in vitro* measurements and 2.0 cm height from *in vivo* measurements, we have used a cylindrical finite element mesh with 1267 nodes and 5328 tetrahedral elements for the 3D reconstruction. Uniform distributions of optical properties that were 30%–50% off the exact values of the background phantom medium were used as the initial guesses for the iterative procedure. The images reported were the results of five iterations when the initial sum of squared errors between measured and computed boundary data reached the steady state with about 1.5 h per iteration in a 600 MHz Pentium III PC.

3 Results and Discussion

Figures 1(b), 1(c), and 1(d) show the reconstructed 3D absorption images at three different cut-planes from the *in vitro* measurements [see Figure 1(a) for the reference coordinate system]. We note that the absorption images show a significant absorption increase in the bone regions relative to the surrounding phantom background. As can be seen, the bone shapes at the joint as well as small structures such as cartilage are imaged.

Figures 3–4 display the optical images at the joint and off-joint planes along *X, Y*, and *Z* directions from the *in vivo* measurements. Figure 3 shows the reconstructed absorption images as a series of transverse slices parallel to the *XOY* plane (see Figure 2 for the reference coordinate system). As can be seen, the bones and several important joint structures can be clearly delineated. The bones and bone/cartilage are imaged, shown in Figures 3(a), 3(b), 3(e), and 3(f). Small structures such as blood vessels and extensor tendons are differentiated in Figures 3(b) and 3(c). The synovium is also identified [Figure 3(d)]. To view the bones and joint at differ-
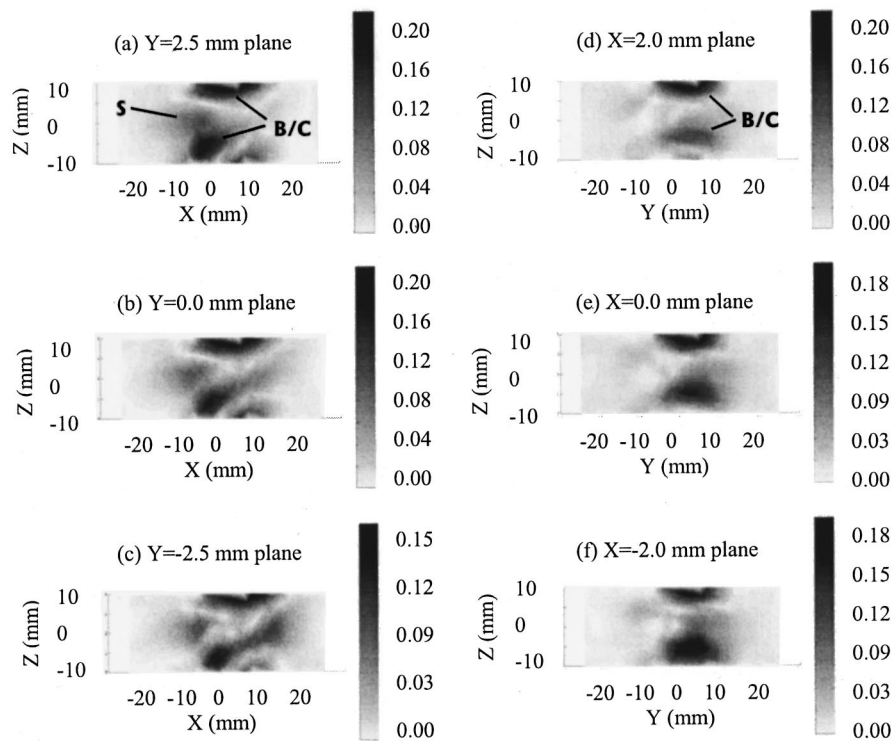
Fig. 4 Longitudinal slices of reconstructed absorption images from *in vivo* measurements obtained around the PIP joint of the index finger (the dark region corresponds to the finger; the gray background corresponds to the solid phantom). The axes (left and bottom) illustrate the spatial scale, in millimeters, whereas the gray scale (right) records the absorption coefficient, in inverse millimeters. *B/C*: bone/cartilage; *S*: synovium.

ent directions, we have provided series of images in Figure 4, at cut-planes parallel to *XOZ* and *YOZ*, respectively. Due to the strong absorption of the bones some joint structures cannot be seen in these longitudinal images, but the appearances of the bones, cartilage, synovium, and blood vessel are evident.

It is interesting yet important to examine these absorption images shown in Figures 3–4 in terms of the absorption coefficient of each structure reconstructed, because the clinical potential of DOT would mostly lie on the difference of the optical properties between diseased and healthy bone/joint tissues. For example, an osteoporosis patient may show changed optical properties in the bone, while a rheumatoid arthritis patient may have increased optical properties in the synovium.[38–41] The average absorption coefficients of bone and cartilage from our images are calculated to be 0.18 and 0.04/mm, respectively, which are in excellent agreement with the reported values of 0.15–0.18/mm for human bone[41] and 0.033/mm for rabbit cartilage.[42] The average absorption coefficient of synovium is found to be 0.094/mm, which is also in excellent agreement with that reported in the literature.[39,40] The average absorption coefficients of blood vessels and tendons are approximately 0.056 and 0.044/mm, respectively. We note that the recovered absorption coefficient of the surrounding phantom background is 0.0054/mm which is about 8% off its exact value.

It is also important to recognize some of the advantages that 3D DOT has over 2D DOT. In our previous 2D images,[29] critical joint structures such as synovium, cartilage, blood vessel, and tendon cannot be delineated. In addition, the 2D im-

ages have significantly underestimated the absorption coefficient of bones. In terms of the imaging resolution, objects as small as 1–2 mm in diameter such as the blood vessels are clearly identified from the 3D images presented which is typical for imaging a 5 cm diameter phantom/finger sample using DOT. We believe that if smaller core diameter fibers were used so that the source/detector fiber probe could directly contact the finger joints without using a large volume of phantom materials, the imaging resolution would be improved. We plan to perform such studies in the near future. In Figure 4, we have also noticed some boundary effects at the top and bottom edges in the bone regions. This was caused most probably by the strong absorption and scattering of the bones within the limited volume measured. We can increase the measuring volume to minimize this boundary impact on the region of interest.

In summary, we have demonstrated *in vivo* that bone and joint tissues can be imaged by 3D DOT. To the best of our knowledge, this study presents the first report of quantitative absorption images of *in vitro* and *in vivo* bones/joints that were obtained by using three-dimensional diffuse optical tomography with model-based image reconstruction methods.

References

1. A. Yodh and B. Chance, "Spectroscopy and imaging with diffusing light," *Phys. Today* **48**, 34–40 (1995).
2. S. Colak, M. van der Mark, G. tHooft, J. Hoogenraad, E. van der Linden, and F. Kuijpers, "Clinical optical tomography and NIR spectroscopy for breast cancer detection," *IEEE J. Sel. Top. Quantum Electron.* **5**, 1143–1158 (1999).
3. V. Ntziachristos, A. Yodh, M. Schnall, and B. Chance, "Concurrent MRI and diffuse optical tomography of breast after indocyanine green enhancement," *Proc. Natl. Acad. Sci. U.S.A.* **97**, 2767–2772 (2000).
4. B. W. Pogue, S. P. Poplack, T. O. McBride, W. A. Wells, K. S. Osterman, U. L. Osterberg, and K. D. Paulsen, "Quantitative hemoglobin tomography with diffuse near-infrared spectroscopy: pilot results in the breast," *Radiology* **218**, 261–266 (2001).
5. H. Jiang, N. Iftimia, J. Eggert, L. Baron, K. Klove, Y. Xu, Y. Yang, and T. Pope, "Near-infrared optical imaging of breast," *Acad. Radiol.* (in press).
6. D. A. Benaron, P. R. Contag, and C. H. Contag, "Imaging brain structure and function, infection and gene expression in the body using light," *Philos. Trans. R. Soc. London, Ser. B* **352**, 755–761 (1997).
7. B. Chance, E. Anday, S. Nioka, S. Zhou, L. Hong, K. Worden, C. Li, T. Murray, Y. Ovetsky, D. Pidikiti, and R. Thomas, "A novel method for fast imaging of brain function, non-invasively, with light," *Opt. Express* **2**, 411–423 (1998).
8. J. R. Singer, F. A. Grunbaum, P. Kohn, and J. P. Zubelli, "Image reconstruction of the interior of bodies that diffuse radiation," *Science* **248**, 990–993 (1990).
9. R. L. Barbour, H. Graber, R. Aronson, and J. Lubowsky, "Model for 3D optical imaging of tissue," in *Proc. 10th Annual Int. Geoscience Remote Sensing Symp.*, Vol. II, pp. 1395–1399 (1990).
10. S. R. Arridge, M. Schweiger, and D. T. Delpy, "Iterative reconstruction of near infra-red absorption images," *Proc. SPIE* **1767**, 372–383 (1992).
11. M. A. O'Leary, D. A. Boas, B. Chance, and A. G. Yodh, "Experimental images of heterogeneous turbid media by frequency-domain diffusing-photon tomography," *Opt. Lett.* **20**, 426–428 (1995).
12. H. Jiang, K. D. Paulsen, U. L. Osterberg, B. W. Pogue, and M. S. Patterson, "Simultaneous reconstruction of absorption and scattering maps in turbid media from near-infrared frequency-domain data," *Opt. Lett.* **20**, 2128–2130 (1995).
13. S. B. Colak, D. Papaioannou, G. tHooft, M. van der Mark, H. Schomberg, J. Paasschens, J. Melissen, and N. van Asten, "Tomographic image reconstruction from optical projections in light diffusing media," *Appl. Opt.* **36**, 180–213 (1997).
14. S. A. Walker, S. Fantini, and E. Gratton, "Image reconstruction by backprojection from frequency-domain optical measurements in highly scattering media," *Appl. Opt.* **36**, 170–179 (1997).
15. R. L. Barbour, H. Graber, Y. Wang, J. Chang, and R. Aronson, "Perturbation approach for optical diffusion tomography using continuous-wave and time-resolved data," *Medical Optical Tomography: Functional Imaging and Monitoring*, G. Muller, Ed., pp. 87–120, SPIE, Bellingham, Washington (1993).
16. J. Schotland, J. Haselgrove, and J. Leigh, "Photon hitting density," *Appl. Opt.* **32**, 448–453 (1993).
17. X. Li, T. Durduran, A. Yodh, B. Chance, and D. Pattanyak, "Diffraction tomography for biochemical imaging with diffuse-photon density waves," *Opt. Lett.* **22**, 573–575 (1997).
18. C. Matson and H. Liu, "Analysis of the forward problem with diffuse photon density waves in turbid media by use of a diffraction tomography model," *J. Opt. Soc. Am. A* **16**, 455–466 (1999).
19. X. Chen and D. Boas, "Diffuse optical reflection tomography with continuous-wave illumination," *Opt. Express* **3**, 118–123 (1998).
20. S. R. Arridge and M. Schweiger, "Image reconstruction in optical tomography," *Philos. Trans. R. Soc. London, Ser. B* **352**, 717–728 (1997).
21. A. Hielscher, A. Klose, and K. Hanson, "Gradient-based iterative image reconstruction scheme for time-resolved optical tomography," *IEEE Trans. Med. Imaging* **18**, 262–271 (1999).
22. R. Roy and E. Sevick-Muraca, "Truncated Newton's optimization scheme for absorption and fluorescence optical tomography: Part I Theory and formulation," *Opt. Express* **4**, 353–371 (1999).
23. H. Jiang, K. D. Paulsen, U. L. Osterberg, B. W. Pogue, and M. S. Patterson, "Optical image reconstruction using frequency-domain data: simulations and experiments," *J. Opt. Soc. Am. A* **13**, 253–266 (1996).
24. H. Jiang, K. D. Paulsen, and U. L. Osterberg, "Optical image reconstruction using DC data: simulations and experiments," *Phys. Med. Biol.* **41**, 1483–1498 (1996).
25. H. Jiang, K. D. Paulsen, U. L. Osterberg, and M. S. Patterson, "Frequency-domain optical image reconstruction in heterogeneous media: an experimental study of single-target detectability," *Appl. Opt.* **36**, 52–63 (1997).
26. N. Iftimia and H. Jiang, "Quantitative optical image reconstruction of turbid media using dc measurements," *Appl. Opt.* **39**, 5256–5261 (2000).
27. B. W. Pogue, T. McBride, J. Prewitt, U. Osterberg, and K. Paulsen, "Spatially variant regularization improves diffuse optical tomography," *Appl. Opt.* **38**, 2950–2961 (1999).
28. A. Klose, A. Hielscher, K. Hanson, and J. Beuthan, "Two- and three-dimensional optical tomography of finger joints for diagnostics of rheumatoid arthritis," *Proc. SPIE* **3566**, 151–159 (1998).
29. Y. Xu, N. Iftimia, H. Jiang, L. Key, and M. Bolster, "Imaging of *in vitro* and *in vivo* bones and joints with continuous-wave diffuse optical tomography," *Opt. Express* **8**, 447–451 (2001).
30. H. Jiang, N. Iftimia, Y. Xu, L. Key, and M. Bolster, "*In vivo* detection of osteoarthritis with diffuse optical tomography," IEEE J. Sel. Top. Quantum Electron. (submitted).
31. H. Jiang, "Three-dimensional optical image reconstruction: Finite element approach," in *Proc. Advances in Optical Imaging and Photon Migration*, Optical Society of America, pp. 156–158 (1998).
32. M. Schweiger and S. Arridge, "Comparison of two- and three-dimensional reconstruction methods in optical tomography," *Appl. Opt.* **37**, 7419–7428 (1998).
33. M. Eppstein, D. Dougherty, D. Hawrysz, and E. Sevick-Muraca, "Three-dimensional optical tomography," *Proc. SPIE* **3597**, 97–105 (1999).
34. H. Jiang, Y. Xu, and N. Iftimia, "Experimental three-dimensional optical image reconstruction of heterogeneous turbid media," *Opt. Express* **7**, 204–209 (2000).
35. S. Arridge, "A method for three-dimensional time-resolved optical tomography," *Int. J. Imaging Syst. Technol.* **11**, 2–11 (2000).
36. M. J. Holboke, B. Tromberg, X. Li, N. Shah, J. Fishkin, D. Kidney, J. Butler, B. Chance, and A. Yodh, "Three-dimensional diffuse optical mammography with ultrasound localization in a human subject," *J. Biomed. Opt.* **5**, 237–247 (2000).
37. H. Jiang, Y. Xu, N. Iftimia, L. Baron, and J. Eggert, "Three-dimensional optical tomographic imaging of breast in a human subject," *IEEE Trans. Med. Imaging* (in press).
38. V. Prapavat, R. Schuetz, W. Runge, J. Beuthan, and G. Muller, "*In vivo* investigations on the detection of chronical polyarthritis using a cw transillumination method at interphalangeal joints," *Proc. SPIE* **2626**, 360–366 (1995).
39. J. Beuthan, V. Prapavat, R. Naber, O. Minet, and G. Muller, "Diagnostic of inflammatory rheumatic diseases with photon density waves," *Proc. SPIE* **2676**, 43–53 (1996).
40. V. Prapavat, W. Runge, J. Mans, A. Krause, J. Beuthan, and G. Muller, "The development of a finger joint phantom for the optical simulation of early inflammatory rheumatic changes," *Biomedizinische Technik* **42**, 319–326 (1997).
41. J. Beuthan, O. Minet, G. Muller, and V. Prapavat, "IR-diaphanoscopy in medicine," in *Medical Optical Tomography: Functional Imaging and Monitoring*, G. Muller, B. Chance, R. Alfano et al., Eds., pp. 263–282, SPIE Press, Bellingham, Washington (1993).
42. W. F. Cheong, S. Prahl, and A. Welch, "A review of the optical properties of biological tissues," *IEEE J. Quantum Electron.* **26**, 2166–2185 (1990).